



HAL
open science

Detector-electrode for alpha spectrometry in water sample, numerical and early feasibility investigation toward thermocompression bonding assembly process

N. Schmitt, S. Colas, N. Saurel, F. Bassignot, B. Vuillemin, Jean-Emmanuel Groetz

► To cite this version:

N. Schmitt, S. Colas, N. Saurel, F. Bassignot, B. Vuillemin, et al.. Detector-electrode for alpha spectrometry in water sample, numerical and early feasibility investigation toward thermocompression bonding assembly process. Nuclear Instruments and Methods in Physics Research Section A: Accelerators, Spectrometers, Detectors and Associated Equipment, 2020, 953, pp.163270. 10.1016/j.nima.2019.163270 . hal-03549016

HAL Id: hal-03549016

<https://hal.science/hal-03549016>

Submitted on 11 Feb 2022

HAL is a multi-disciplinary open access archive for the deposit and dissemination of scientific research documents, whether they are published or not. The documents may come from teaching and research institutions in France or abroad, or from public or private research centers.

L'archive ouverte pluridisciplinaire **HAL**, est destinée au dépôt et à la diffusion de documents scientifiques de niveau recherche, publiés ou non, émanant des établissements d'enseignement et de recherche français ou étrangers, des laboratoires publics ou privés.

Copyright

Detector-electrode for alpha spectrometry in water sample, numerical and early feasibility investigation toward thermocompression bonding assembly process

N. Schmitt^{a,b}, S. Colas^b, N. Saurel^b, F. Bassignot^c, B. Vuillemin^d, J.E. Groetz^a

^a*Laboratoire Chrono-Environnement, UMR CNRS 6249, Université de Bourgogne Franche-Comté,
F-25030 Besançon, France*

^b*CEA/Valduc, F-21120 Is-sur-Tille, France*

^c*FEMTO Engineering, 15B avenue des Montboucons, F-25030 Besançon, France*

^d*Institut Carnot de Bourgogne, UMR CNRS 6303, Université de Bourgogne Franche-Comté, F-21078
Dijon, France*

Abstract

This study focuses on the feasibility of a detector-electrode for direct alpha measurement in aqueous samples. Such a device could be made by adding a boron doped diamond electrode on top of a standard silicon detector, with bonding and insulating layers. The impact of these different layers has been investigated by Monte-Carlo simulation (MCNP6), to find a compromise between alpha detection of the silicon, electrode and shielding properties of the diamond. The assembly process involving thermocompression between both substrates was successfully achieved under a clean room conditions.

Keywords: Alpha particle spectrometry, CVD diamond, Electrode, Monte-Carlo simulation, Thermocompression bonding, Silicon detector

1. Introduction

2 In the field of nuclear measurement, alpha particle spectrometry is used to identify
3 radionuclides, mainly actinides, and to quantify them through their activity. It is carried
4 out usually by using two different methods which require several chemical processes for
5 the separation of radionuclides, in order to generate a radioactive source. A common
6 method involves deposition of radionuclides of interest on a disc, whose the identification

7 and quantification are measured in a vacuum chamber. The radioactive source should be
8 as thin as possible in order to prevent energy loss and straggling by self-absorption and to
9 identify alpha-emitting radionuclides by energy discrimination in the energy spectrum.
10 This identification is performed through the centroid of peaks and the area beneath
11 the peaks corresponds to the total activity of radionuclides. As a second method, al-
12 pha counting could be performed with organic liquid scintillators, with a high counting
13 efficiency [1].

14 In the family of semiconductor detectors, the passivated planar detectors are the most
15 used for alpha activity monitoring and radionuclides identification in the environment.
16 The PIPS[®] detectors (Passivated Ion implant Planar Silicon) used in alpha spectrometry
17 can not withstand an aggressive chemical and acid solution such as in nuclear effluents,
18 making these detectors unappropriated for a direct measurement in situ [2], which would
19 require to overlay the PIPS[®] with a protective material [3]. As a potential candidate,
20 diamond materials exhibit radiation hardness and chemical inertness properties. These
21 properties made it possible for polycrystalline diamond to be successfully used as an
22 immersed detector of alpha particles in a concentrated plutonium solution in nitric acid
23 (2 mol l^{-1}), with a ^{239}Pu concentration ranging from 10 to 100 mg l^{-1} [4]. In this
24 configuration, the path length of the alpha track before reaching the detector corresponds
25 to the thickness of the liquid crossed by alpha particles, limited by their range in water,
26 i.e. a few tens of micrometer. This technique can only measure active material close to
27 the detector. In particular, it is suitable for real-time extremely high activity levels but
28 not for monitoring low activities in water.

29 After this early success, diamond detector was improved by the use of synthetic di-
30 amond as an active alpha-detector [5–9]. High quality diamond film can be produced
31 by chemical vapor deposition (CVD) from a carbon precursor such as CH_4 or CO_2 and
32 hydrogen. The carbon species and hydrogen must be activated since at low pressure,
33 graphite is thermodynamically stable, and without activation, only graphite would be
34 formed. Activation can be obtained at high temperature with a hot filament heated up
35 to 2600 K, then atomic hydrogen is formed and the carbon species become activated
36 in the vicinity of the hot metal. This method made possible the formation of poly-
37 crystalline CVD diamond on large areas. Nucleation is a critical phase in the diamond

38 deposition process due to its strong influence on film roughness and pinhole formation.
39 The substrate surface must be treated before deposition to achieve a high nuclei den-
40 sity. As the temperature of the process is around 800-900°C and high nuclei density is
41 easier to achieve on carbide-forming material, diamond films are generally deposited on
42 silicon-based material (Si, SiC, Si₃N₄) or refractory metals and alloys [10].

43 In order to perform direct alpha spectrometry in a liquid sample, a preliminary work
44 suggested combining the detection properties of a PIPS[®] detector with the diamond
45 shielding and electrode properties to develop an hybrid Si-diamond detector electrode.
46 This type of detector has been manufactured by de Sanoit et al. with a process of
47 boron doped diamond chemical vapor deposition on the surface of a commercial PIPS[®]
48 detector [11, 12]. The process consists in depositing actinides using an electrochemical
49 technique directly onto the surface of the boron doped entrance window of the alpha
50 detector, acting as a cathode [13, 14]. Then, the alpha activity of the deposited actinides
51 could be measured by the PIPS[®] detector.

52 However, the high temperature required in the diamond CVD process on silicon
53 substrates could significantly reduce the detection properties of the PIPS[®] diode. The
54 diffusion of implanted ions in silicon increases the dead zone of the diode, which could
55 impact on the path of alpha particles before reaching the active part of the detector. In
56 order to prevent this major drawback, it is imperative to avoid thermal processes and
57 another method should be investigated.

58 The use of a metal layer such gold or indium as a bonding layer between two materials
59 could be an attractive alternative [15]. The application of such an innovative process will
60 be a real breakthrough to the fabrication of a detector electrode. For this aim, the
61 impact of the different layers and the feasibility of bonding a diamond electrode on a
62 silicon detector has been studied. Monte-Carlo simulation has been used to design the
63 new silicon detector by investigating the influence of the shielding, bonding, insulating
64 and source layers on the detection properties over a range of alpha particle energies from
65 4 to 5.5 MeV. Afterwards, a preliminary feasibility study has been realised, followed by
66 the development of the fabrication process using boron doped diamond electrode and
67 silicon detector.

68 **2. Material, device and simulation**

69 *2.1. Material*

70 *2.1.1. Electroprecipitation and source deposition*

71 In order to carry out in situ direct measurements in effluents, the surface of the
72 detector should be in contact with the liquid sample containing the radionuclides. In
73 this configuration, an actinide electroprecipitation can be realised to form a radioactive
74 source on the detector surface. Such a method involves the use of a potential gradient
75 between two electrodes to materialise an hydroxide layer on the cathode surface, which
is the required condition for the actinide precipitation (Fig. 1).

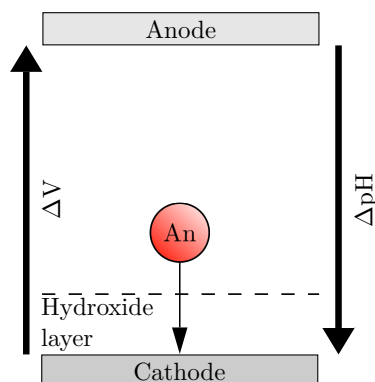


Figure 1: Diagram of the actinide electroprecipitation between two working electrodes.

76

77 In aqueous solution, the range of potential is limited by the electrochemical water
78 decomposition (through the system H_2/H^+ on the reduction side and the system $\text{H}_2\text{O}/\text{O}_2$
79 on the oxidation side). Performing the electrochemical reduction of dissolved oxygen
80 in water (or water reduction) locally modifies the pH near the surface of the working
81 electrode, that results in the formation of a base layer (pH 10-11 for the dissolved oxygen
82 reduction, pH 12-13 for the water reduction). Increasing the pH of an aqueous solution
83 containing actinide ions changes the structure of these ions: protons are expelled from
84 the internal hydration sphere. In this way, the actinide ions accumulate hydroxyl ions
85 (OH^-) in the internal sphere and form monohydroxo or polynuclear complexes. As final
86 products, solid hydroxides precipitate on the cathode surface if the solubility product is
87 exceeded [12–14]. As a preliminary study, such a process on a diamond electrode has
88 been performed in a sodium sulfate aqueous solution (0.3 mol l^{-1} , $\text{pH}= 4$) for a thorium

89 concentration of 10^{-3} mol l $^{-1}$. The experiment was carried out inside a laminar mixing
 90 cell of 300 ml, using chronoamperometry method with an applied voltage of -1 V during
 91 20 hours. After drying, a yellow deposition was observed on the surface of the diamond
 92 electrode (Fig 2, left) and the thorium was identified by gamma spectrometry through
 93 its progenies, ^{228}Ac , ^{212}Pb and ^{208}Tl (Fig. 2, right).

94 It should be noted that this deposition was obtained after stopping the electropre-
 95 cipitation and evaporating the solution. So, the exact composition of the actinide gel
 96 formed at the electrode surface in the solution is not very well known, together with
 97 its thickness and density. Therefore, the radioactive source was supposed homogeneous,
 98 with a density similar to that of water.

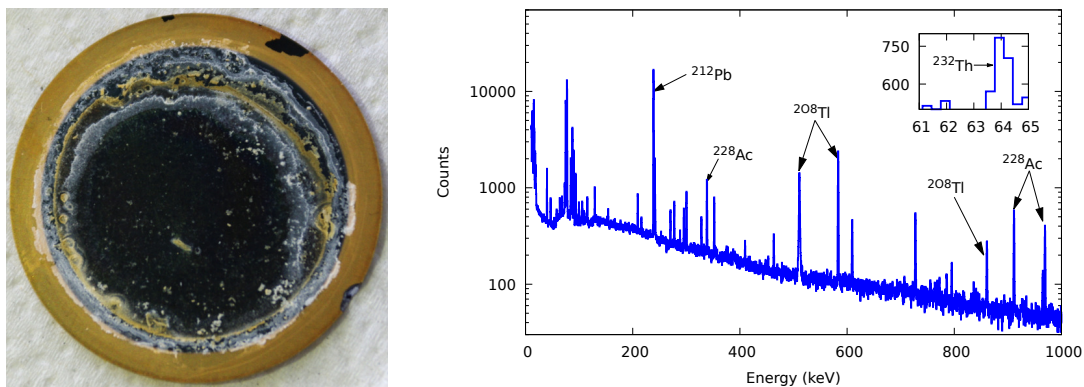


Figure 2: Left: Thorium deposited on the surface of a boron doped diamond electrode. Right: Gamma spectrum of thorium deposited on the boron doped diamond electrode.

99 2.1.2. Detector

100 The detector investigated has been approximated by a slab of pure silicon with a
 101 2.54-cm diameter and 300- μm thickness with a density of 2.33 g cm $^{-3}$, on top of which
 102 a diamond electrode of the same area is bonded with a Ti-Au layer. This bonding layer
 103 is composed of:

- 104 • 100 nm of gold with a density of 19.30 g cm $^{-3}$,
- 105 • 50 nm of titanium with a density of 4.51 g cm $^{-3}$. The use of Ti in the bonding
 106 layer facilitates Au adhesion on Si and SiO $_2$.

107 In the assembly process, this bonding layer is deposited on both parts, i.e. on the PIPS[®]

108 detector and on the diamond electrode.

109

110 As for the diamond electrode, it is made up of two different layers:

- 111 • the electrical insulating layer : silicon oxide SiO_2 with 500-nm thick with a density
112 of 2.65 g cm^{-3} , and a silicon nitride Si_3N_4 with 200-nm thick with a density of 3.44
113 g cm^{-3} , used in the diamond chemical vapor deposition process to strengthen the
114 adhesion of the diamond layer on SiO_2 .
- 115 • the shielding layer is a polycrystalline diamond electrode with a density of 3.52 g
116 cm^{-3} and doped with boron at around 8000 ppm, with an optimal thickness which
117 was investigated by Monte-Carlo simulation.

118 Without information on the energy resolution, the simulated detector is supposed
119 ideal.

120 Fig. 3 shows the stacking of all different layers, corresponding to the different config-
121 urations of the detector:

- 122 • bare Si diode, corresponding to the PIPS[®] detector,
- 123 • PIPS[®] detector with the electrical insulating layer ($\text{SiO}_2/\text{Si}_3\text{N}_4$)
- 124 • PIPS[®] detector with the insulating layer and the shielding layer in CVD diamond.
125 This configuration would correspond to the growth of CVD diamond on the PIPS[®]
126 detector, which was the first process investigated by de Sanoit et al.
- 127 • PIPS[®] detector with the bonding layer of Ti/Au for the assembly with the insu-
128 lating layer and the CVD diamond. The last diagram corresponds to this project
129 with a gold layer for the bonding of the diamond electrode on the Si diode. The
130 use of Ti in the bonding layer facilitates Au adhesion on Si and SiO_2 .

131 2.2. Monte-Carlo simulation

132 The MCNP6 (Monte-Carlo N-Particle) code [18] was used to model the detector
133 with the different added layers and a radioactive water source, with a density of 1 g
134 cm^{-3} , in accordance with section 2.1.1. The considered case uses an aqueous solution

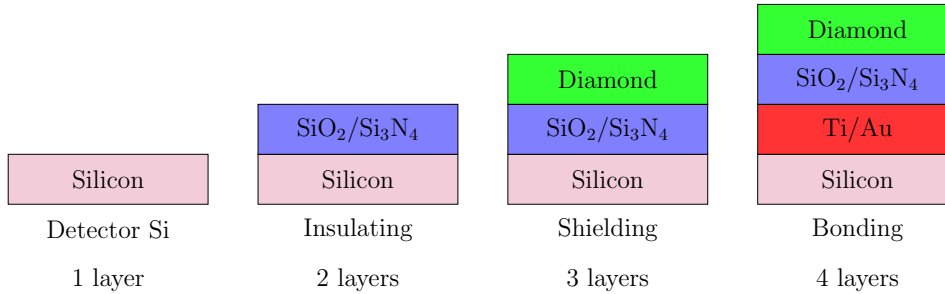


Figure 3: Diagram (not to scale) of the different slabs used to study the impact of the coating layers on alpha particle measurement.

135 containing diluted ^{241}Am (5.49 MeV) for a mono energetic source, as well as ^{241}Am ,
 136 ^{239}Pu (5.16 MeV) and ^{235}U (4.40 MeV) for a multi energetic source. Alpha particles
 137 were generated randomly throughout the volume of the simulated source, with an energy
 138 cut-off lowered to 1 keV. The observable or estimator, called tally in MCNP6, used for
 139 modelling the detector response is the F8 tally, which provides the pulse height created by
 140 alpha particles in the detector. Each run used 10^6 alpha particle as histories (one history
 141 is the complete description for one particle of its transport and interactions through
 142 matter) and the uncertainties on the number of counts were about 1.1%.

143 Energy loss for alpha particles is directly linked to the stopping power in every mate-
 144 rial (Fig. 4). Monte-Carlo simulation enables to take into account the energy and range
 145 straggling, behind the spread of energies after the monoenergetic alpha particles pass
 146 through a given thickness of material slab [1].

147 3. Simulation results

148 3.1. Influence of the diamond layer thickness

149 The constraints for the thickness of the diamond layer concern mainly the limitation
 150 of the particle energy attenuation, the modification of peak shape (width and height) and
 151 the conservation of the diamond properties as electrode. The thickness for the diamond
 152 layer investigated ranges from 0.1 to 1 μm , corresponding to the minimal deposited thick-
 153 ness achievable by the industrial partner, NeoCoat (La Chaux-de-Fonds, Switzerland),
 154 and an arbitrary maximum source thickness until total attenuation of alpha particles by
 155 the diamond layer.

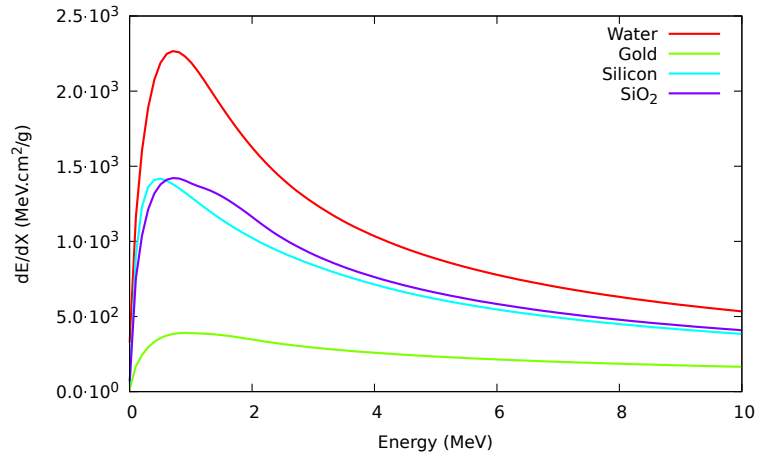


Figure 4: Stopping power of water, gold, silicon and silicon dioxide normalized to their densities [17].

156 As Fig. 5 shows, the peak shape does not change from 0.1 μm , but the energy
 157 of the incident alpha particle shifts linearly to the lower energies and the height of the
 158 peak decreases. During its path in diamond, the energy of the incident alpha particle
 159 is attenuated. The thicker the diamond, the more the particle loses energy during its
 160 crossing. Increasing the thickness of the diamond layer broadens the peak. For such a
 161 thickness, the surface roughness, typically between 10 and 30 nm, could have a weak
 influence on the detection.

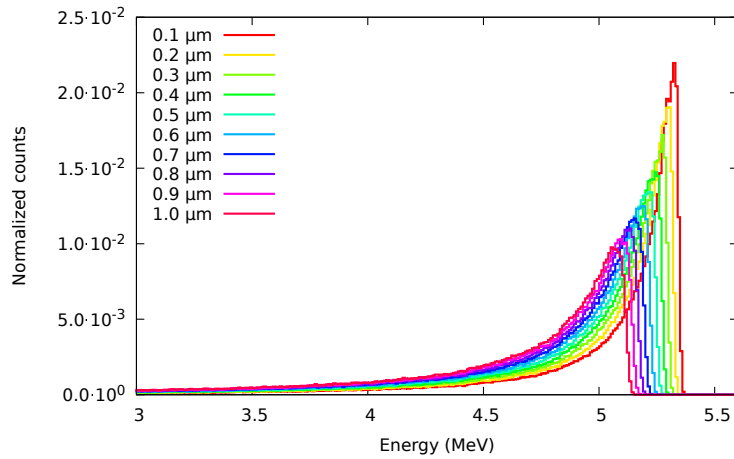


Figure 5: Plot of the simulated alpha spectra as a function of CVD diamond thickness.

162

163 Another parameter to take into account is the resistivity of the electrode: according

164 to the boron doping level, a diamond electrode of 100 nm has approximately a resistivity
 165 of 20 m Ω cm, while a thicker diamond electrode of 1 μ m could reach a resistivity of 5 m Ω
 166 cm, due to the effect of grain boundary. So our choice must be a compromise between
 167 the lower thickness and the best conductivity. In this way, optimal working electrode
 168 properties requires a thickness between 0.3 and 0.4 μ m. For these thicknesses, decrease
 169 in full height was between 31.8% and 42.8%.

170 3.2. Attenuation by insulating, shielding and bonding layers

171 Fig. 6 shows the initial alpha peak on the Si-diode, then with the presence of different
 172 slabs (insulating, bonding and diamond shielding, as shown in Fig. 3). Table 1 gives some
 173 parameter values characterizing the alpha peaks: the centroid, the full height (FH), the
 174 full width at half maximum (FWHM) and the area.

175 For an arbitrarily chosen source thickness of 100 nm, the identification of the most
 176 attenuating layer is possible. In this configuration, the insulating layer shifts the centroid
 177 2.73% to lower energies and attenuates the intensity (FH) 82.45% from those values of
 178 the incident alpha particle in the Si-diode. The shielding and bonding layers provide
 179 respectively an attenuation of 5.85% and 2.21% of the initial FH peak (FH_{Si}). The
 180 insulating layer increases the FWHM from 0.02 MeV to 0.13 MeV, whereas the shielding
 181 layer increases it only from 0.13 to 0.18 MeV and the bonding layer from 0.18 to 0.22 MeV
 182 (Table 1). Attenuations due to the bonding and shielding layers are negligible compared
 183 to the attenuation due to the insulating layer.

Layer	Centroid (MeV)	FH (Normalized counts)	FWHM (MeV)	Normalized peak area	Δ FH/FH _{Si} (%)
Detector (Si – 300 μ m)	5.49	$1.36 \cdot 10^{-1}$	0.02	$4.96 \cdot 10^{-1}$	–
Insulating (SiO ₂ + Si ₃ N ₄ – 700 nm)	5.34	$2.39 \cdot 10^{-2}$	0.13	$4.74 \cdot 10^{-1}$	82.45
Shielding (Diamond – 374 nm)	5.26	$1.59 \cdot 10^{-2}$	0.18	$4.61 \cdot 10^{-1}$	5.85
Bonding (Au+Ti – 150 nm)	5.19	$1.29 \cdot 10^{-2}$	0.22	$4.51 \cdot 10^{-1}$	2.21

Table 1: Characteristics for the simulated alpha peaks according to the different layers.

184 3.3. Source self absorption

185 Controlling the source thickness on the detector surface could be interesting to limit
 186 the self absorption of alpha particles in order to perform a real identification of radionu-
 187 clides in the liquid solution. In this way, a limit of source thickness could be defined,

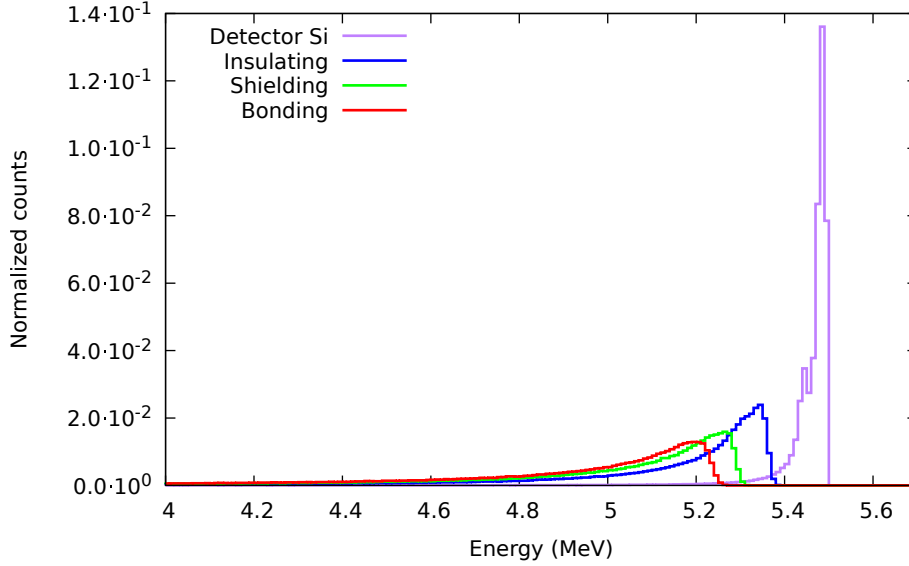


Figure 6: MCNP6 simulation of the alpha spectra for the different detector configurations shown in Fig. 3. The source is $0.1 \mu\text{m}$ thick and it is composed of water containing ^{241}Am , with a density of 1 g cm^{-3} .

188 beyond which the apparent activity remains constant (due to a source thickness greater
 189 than alpha particle path), but mainly because the radionuclide identification could not
 190 be performed in the absence of distinctive peaks.

191 In this configuration, the detector is composed of four different layers described in
 192 section 2.1.2 and Fig. 3, with the CVD diamond slab thickness set to 300 nm .

193 3.3.1. Mono-energetic source

194 For this aim, a mono energetic source, containing ^{241}Am (5.49 MeV), has been simu-
 195 lated. The investigated thickness for the source layer, from $0.1 \mu\text{m}$ to $10 \mu\text{m}$, corresponds
 196 to an ideal source and a more realistic one. The source thickness depends on the time
 197 required by actinide electroprecipitation process as well as the hydrodynamics conditions
 198 inside the cell. The upper thickness corresponds to the alpha particle range at 5.49 MeV
 199 in water and is achievable by micro-fluidic cell or actinide electrodeposition.

200 Fig. 7 and Table 2 show the impact of the source thickness on the peak shape. As the
 201 thickness of the source increases, the height of the peak decreases, also with a growing
 202 broadening. With a thickness between 0.1 and $2 \mu\text{m}$, the peak shape appears to be
 203 well defined. For thicker sources, beyond $2 \mu\text{m}$, the widening of the peak prevents the

204 identification of its centroid, which is a major concern for alpha spectrometry. However,
 205 the simulated activity decreases linearly as the thickness of the source increases. Such
 206 results suggest that the measurement of the global activity could be performed with this
 207 kind of detector without a complete source formation process.

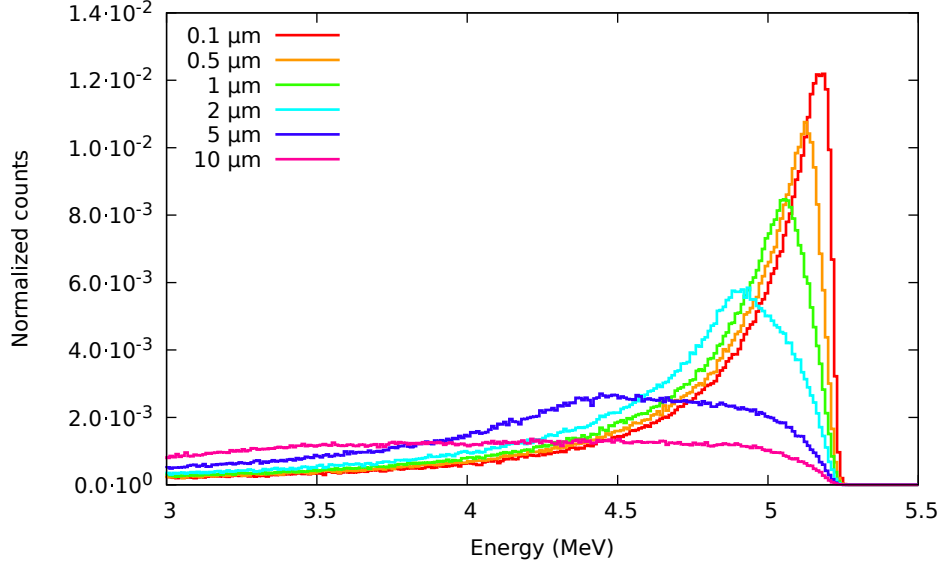


Figure 7: MCNP6 simulation of the impact of the source thickness on alpha measurement.

Source thickness (μm)	Centroid (MeV)	FH (Normalized counts)	FWHM (MeV)	Normalized peak area
0.10	5.18	$1.22 \cdot 10^{-2}$	0.21	$4.63 \cdot 10^{-1}$
0.50	5.12	$1.08 \cdot 10^{-2}$	0.25	$4.59 \cdot 10^{-1}$
1.00	5.05	$8.47 \cdot 10^{-3}$	0.31	$4.53 \cdot 10^{-1}$
2.00	4.93	$5.85 \cdot 10^{-3}$	0.5	$4.43 \cdot 10^{-1}$
5.00	4.44	$2.70 \cdot 10^{-3}$	1.23	$4.11 \cdot 10^{-1}$
10.00	—	$1.36 \cdot 10^{-3}$	—	$3.55 \cdot 10^{-1}$

Table 2: Characteristics of the simulated spectra according to the source thickness.

208 3.3.2. Multi energetic source

209 In the following case, a multi energetic source, containing ^{241}Am (5.49 MeV) ^{239}Pu
 210 (5.16 MeV) and ^{235}U (4.40 MeV) with the same volumetric activity, has been simulated
 211 to investigate the limits for the energy discrimination in such an experimental setup.
 212 Fig. 8 shows the influence of source thickness on the shape of peaks related to the

213 three actinides. For a source thickness between 0.1 and 1 μm , the three peaks remain
 214 identifiable. The thicker the source, the wider the peaks and the centroids of the peaks
 215 shift to lower energies. At 2 μm thick, the peak height is truncated, the discrimination
 216 between the peaks of ^{239}Pu and ^{241}Am begins to be problematic due to the widening
 217 of the FWHM. For a higher source thickness, the distinction between ^{235}U , ^{239}Pu and
 218 ^{241}Am could not be performed, due to the strong self absorption of the source.

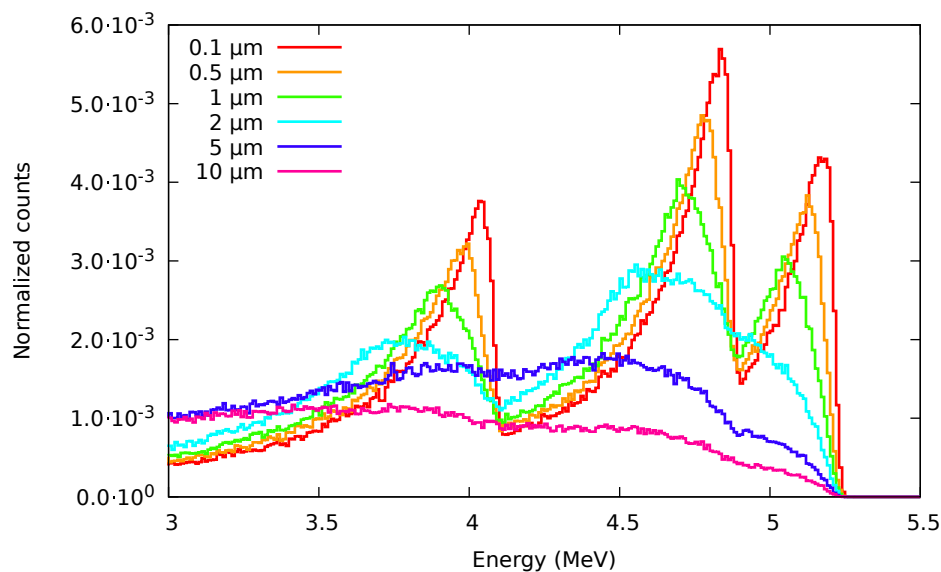


Figure 8: MCNP6 alpha particle spectra for a detector-electrode with different source thicknesses containing ^{241}Am , ^{239}Pu and ^{235}U .

219 4. Feasibility study for assembly

220 4.1. Assembly process

221 Thermocompression bonding at room temperature (15 – 25°C) was studied to as-
 222 semble a boron doped diamond (BDD) electrode on the surface of the silicon detector.
 223 This process involves a clean room technique developed by F. Bassignot *et al* [15]: a thin
 224 layer of titanium/gold was first deposited by sputtering on the surface of both substrates.
 225 These substrates were then pre-bonded by mechanical compression of their metallized
 226 surfaces into a wafer bonding machine (EVG 501). Once the pre-bonding was done, the
 227 bonding process was completed by applying a strong pressure to the stack with an hy-

228 draulic press. This last step should remove most of gluing defects due to surface flatness,
229 total thickness variation and bow/wrap defects.

230 For this method, polished surfaces of optical quality were necessary to assure the
231 bonding of the different substrates. A surface roughness of 30 nm and 1 nm were respec-
232 tively measured for the diamond layer and the silicon detector. The measured surface
233 roughness for both materials is lower than the limit of 80 nm required for a successful
234 thermocompression bonding.

235 We remind that the electrode structure is composed of a boron doped diamond on a
236 $\text{Si}_3\text{N}_4/\text{SiO}_2$ layer on a pure silicon wafer, with a total thickness around 1 μm . Due to
237 the impossibility of handling such a thin material, the simplest way was to deposit on
238 the free diamond surface an insulating layer, eroding the SiO_2 layer to have a surface
239 roughness of 10 nm and then depositing the bonding layer of Ti/Au. Finally, the initial
240 layers $\text{SiO}_2/\text{Si}_3\text{N}_4$ and Si wafer, on which the CVD diamond growth was made, had to
241 be removed (section 4.3).

242 4.2. Bonding tests

243 Separate preliminary adhesion tests of the thermocompression bonding layer were
244 performed, for a diamond electrode and a pure silicon wafer (electrode-Si wafer), for
245 a PIPS[®] detector and a pure silicon wafer (detector-Si wafer). The strength of the
246 bonding was investigated by performing tearing test on the silicon layer with a tweezer
247 and mechanical engraving. The electrode-Si wafer bonding was good enough to resist
248 mechanical engraving. The detector-Si wafer bonding was not satisfying, due to the
249 convexity of the detector surface. Removing the detector from its casing reduced the
250 pressure applied on it and also its convexity, which enabled a satisfactory bonding on a
251 silicon wafer (Fig. 9).

252 The final test was for the assembly of the electrode and the PIPS[®] detector (electrode-
253 detector). Sticking the BDD on the detector surface required the deposition of a $\text{Si}_3\text{N}_4/\text{SiO}_2$
254 layer on the BDD surface, then mechanically polished to clear surface defects of the
255 electrode. After this intermediate step, the detector-electrode bonding was successfully
256 achieved (Fig. 10).

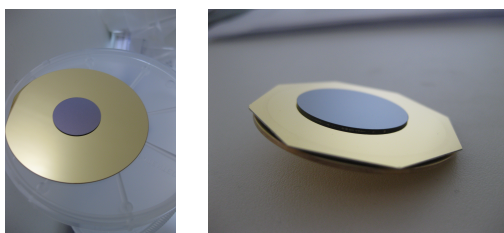


Figure 9: BDD electrode bonded on top of a silicon wafer (left) and silicon wafer bonded on top of the detector (right)

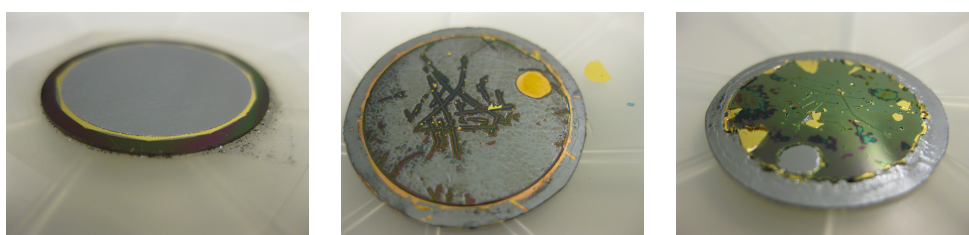


Figure 10: BDD electrode bonded on top of a PIPS[®] detector with gold (100 nm) and titanium (50 nm). Left: After mechanical etching. Middle: After etching with KOH. Right: After etching with HF–HNO₃.

257 4.3. Surface etching

258 Once the bonding completed, the etching process of the electrode surface layer was
 259 necessary to release the detector active aperture from the original silicon substrate of the
 260 BDD. The first step used a mechanical etching to lower the high purity silicon substrate
 261 of the BDD electrode to 50 μm thick. Then the detector has been immersed in a KOH
 262 solution, to remove the silicon substrate without damage on the silica layer. This etching
 263 step has been followed by a mixed solution of hydrofluoric acid (HF) and nitric acid
 264 (HNO₃) to remove the silica and silicone nitride layers above the electrode. Fig. 10 shows
 265 that the KOH did not remove successfully the silicon substrate and that the hydrofluoric
 266 acid was too aggressive and strongly altered the detector surface, the bonding area and
 267 the diamond electrode. Hydrofluoric acid behaves like a gas, the presence of defects at
 268 the interface gold-material or Au-Au promotes its diffusion through the material, thus
 269 resulting in these unwanted damages (Fig. 10).

270 5. Discussion

271 A 0.3 to 0.4 μm thin shielding layer of diamond material on top of a standard PIPS[®]
 272 detector would have a limited impact with regard to the alpha spectrometry properties

273 of the device (Fig. 5). However, the insulating layer, required to perform both actinide
274 electro-chemically assisted precipitation and alpha spectrometry, reduces the detection
275 properties of the detector-electrode (Fig. 6). In those cases, a 0.1 μm thick source has
276 been simulated, that corresponds to an ideal source. The thickness of the source could
277 impact significantly the quality of the alpha spectra, since a ^{241}Am source emits alpha
278 particles that are detected at energies below 4 MeV (Fig. 7). Below a source thickness
279 of 2 μm , the peaks from ^{235}U , ^{239}Pu and ^{241}Am could be identifiable for an alpha multi-
280 energetic source. Above 2 μm , signals from ^{235}U and ^{239}Pu are completely hidden by
281 the signal from ^{241}Am (Fig. 8).

282 The feasibility study revealed that the detector and the electrode surfaces are not
283 perfectly flat. The thermal process used to produce CVD diamond and silicon detector
284 was responsible of this significant drawback. On the other hand, the pressure applied
285 in its case was causing the convexity of the detector. Opening the case of the PIPS[®]
286 detector allowed to reduce this problem and successfully perform thermocompression
287 bonding with a Ti-Au layer between diamond electrode and silicon detector (Fig. 9).

288 The surface etching with hydrofluoric acid was too aggressive for the detector (Fig. 10).
289 To prevent this, a dry etching process was chosen and a plasma etching process is thus
290 under study. It allowed to reach a remaining thickness of 1.6 μm on the surface of the
291 diamond electrode.

292 6. Conclusion

293 The feasibility of a new alpha detector-electrode, combining Si diode and CVD di-
294 amond assembled by thermocompression, and its impact on detection properties were
295 investigated. To preserve the boron doped diamond shielding and electrode properties
296 with a low attenuation of the incident alpha particle energy, the diamond thickness should
297 be kept between 300 nm and 400 nm. The insulating layer is responsible for most of the
298 attenuation in the energy of alpha particles. On the other hand, the contribution of
299 the bonding layer on attenuation could be neglected. For an ideal detector in terms of
300 resolution and an homogeneous source thinner than 2 μm , the identification of alpha
301 emitters with similar volumetric activities could be performed. Such conditions could be
302 achieved by performing actinides electrodeposition in a well-mixed aqueous solution.

303 Concerning the assembly process, thermocompression of diamond electrode on the sili-
304 con detector surface was successfully achieved without visible damage on both substrates.
305 However, this process requires a roughness under 10 nm and can only be performed in
306 clean room conditions. As releasing the active window is still under development, other
307 experiments are focused on the dry attack of the diamond substrates.

308 **Acknowledgement**

309 The authors would like to thank Christophe Provent and David Rats from NeoCoat,
310 La Chaux-de-Fonds – Switzerland (<http://www.neocoat.ch>), for the valuable discussions
311 and supplying the diamond electrodes.

312 **References**

- 313 [1] G.F. Knoll, Radiation Detection and Measurement, 4th edition, Wiley, Hoboken (NJ), 2010.
314 [2] F. Amoudry, P. Burger. Determination of the $^{239}\text{Pu}/^{240}\text{Pu}$ isotopic ratio by high resolution alpha
315 spectrometry, Nuclear Instruments and Methods in Physics Research 232 (2) (1984) 360 - 367.
316 [3] T.R. Garcia, B. Reinke, W. Windl, T.E. Blue, Alpha spectroscopy for *in-situ* liquid radioisotope
317 measurements, Nucl. Instrum. Methods Phys. Res. A 780 (2015) 119-126.
318 [4] S.F. Kozlov, E.A. Konorova, M.I. Krapivi, V.A. Nadein, V.G. Yudina, Usage of diamond detectors
319 as immersed alpha-counters, IEEE Transactions on Nuclear Science 24 (1977) 242-243.
320 [5] E.-K. Souw, R.J. Meilunas. Response of CVD diamond detectors to alpha radiation. Nucl. Instrum.
321 Methods Phys. Res. A 400 (1997) 69-86.
322 [6] P. Bergonzo, F. Foulon, A. Brambilla, D. Tromson, C. Jany, S. Haan. Corrosion hard CVD diamond
323 alpha particle detectors for nuclear liquid source monitoring, Diamond and Related Materials 9 (3)
324 (2000) 1003-1007.
325 [7] F. Schirru, D. Chokheli, M. Kiš. Thin single crystal diamond detectors for alpha particle detection.
326 Diamond and Related Materials 49 (2014) 96-102.
327 [8] J.A. Dueñas, J. de la Torre Pérez, A. Martín Sánchez, I. Martel. Diamond detector for alpha-particle
328 spectrometry. Applied Radiation and Isotopes 90 (2014) 177-180.
329 [9] Z. Zhang, J. Huang, Y. Xi, X. Zhou, K. Tang, Y. Xia, Y. Lu, CVD diamond film detectors for
330 alpha particles with a new electrode structure of reduced graphene oxide/Au, Materials Science in
331 Semiconductor Processing 91 (2019) 260-266.
332 [10] NeoCoat SA, Diamond coating and CVD technologies, available at <http://www.neocoat.ch> (ac-
333 cessed on June 18th, 2019).
334 [11] J. de Sanoit, C. Mer-Calfati, M. Pomorski. Détecteur alpha électrochimique assisté pour la mesure
335 nucléaire en milieu liquide et procédé associé. FR2965936-A1, 2010.
336 [12] J. de Sanoit, T. Q. Tran, M. Pomorski, S. Pierre, C. Mer, P. Bergonzo. Design of an electrochemically
337 assisted radiation sensor for alpha-spectrometry of actinides traces in water. Applied Radiation and
338 Isotopes 80 (2013) 32-41.
339 [13] Q. T. Tran, M. Pomorski, de Sanoit. Optimization of Actinides Trace Precipitation on Diamond/Si
340 PIN Sensor for Alpha-Spectrometry in Aqueous Solution. IEEE Transactions on Nuclear Science
341 61 (2014) 2081-2089.
342 [14] J. de Sanoit, C. Mer-Calfati, M. Pomorski. Detection method using an electrochemically-assisted
343 alpha detector for nuclear measurement in liquid medium. EP2625457 B1, 2015.
344 [15] F. Bassignot, E. Courjon, G. Ulliac, S. Ballandras, J-M. Lesage, R. Petit. Acoustic resonator based
345 on periodically poled transducers: Fabrication and characterization. Journal of Applied Physics
346 112, 074108 (2012).
347 [16] A. Diener, C. Wilhelm. Test of a novel sensor for alpha-spectrometry in drinking water matrices.
348 Applied Radiation and Isotopes 103 (2015) 151-159.

- 349 [17] M.J. Berger, J.S. Coursey, M.A. Zucker and J. Chang. Stopping-Power & Range Tables for Elec-
350 trons, Protons, and Helium Ions. NIST Standard Reference Database 124. Last Update to Data
351 Content: July 2017 — NISTIR 4999.
- 352 [18] D.B. Pelowitz, (Ed.), Los Alamos National Laboratory Report LA-CP-11-01708, Los Alamos (2011).